Eur. Phys. J. Plus (2023) 138:970
https://doi.org/10.1140/epjp/s13360-023-04611-z

THE EUROPEAN PHYSICAL JOURNAL PLUS

Regular Article

Thermal effects on the baryon–quark phase transition in hot hybrid neutron stars: a statistical mean-field baryonic model with the standard NJL model for deconfined quarks

S. A. Ghaemmaghami, M. Ghazanfari Mojarrad[a]

Department of Physics, Faculty of Science, University of Kashan, P.O. Box 87317-53153, Kashan, Iran

Received: 10 July 2023 / Accepted: 19 October 2023

Abstract We investigate the thermal effects on the baryon–quark phase transition (PT), utilizing the Maxwell construction (MC) in an isentropic analysis. In order to model the structure and composition of hot hybrid neutron stars (HHNSs) with β-equilibrated dense matter in the presence (absence) of trapped neutrinos, we use a statistical model which agrees with the Thomas–Fermi (TF) approximation for the baryonic phase and the Nambu–Jona-Lasinio (NJL) model for the deconfined quark phase. Our results show that neutrino trapping can provide a considerable softening of the equation of state EOS in the baryon–quark coexistence phase, compared with the situation governed by untrapped (free-streaming) neutrinos. Having a weak dependence on the quark vector coupling constant in the pure quark phase, the temperature meets its maximum value at the threshold baryonic density for the occurrence of the baryon–quark PT. Based on the assumption of the conserved baryonic mass, all of our HHEOS lead to the stable mass structures for a HHNS.

1 Introduction

A core-collapse supernova explosion is considered to be a unique natural laboratory in nuclear astrophysics so that one can test the equation of state (EOS) of hot dense matter to probe the structure and characteristics of a newborn hot neutron star [1–4]. Under such extreme conditions of density and temperature, the baryon–quark phase transition (PT) is expected to occur inside the stellar core, leading to the formation of a hot hybrid neutron star (HHNS) [5–14]. Over the last few decades, the theoretical approaches have been vastly developed in describing the EOS of baryonic [15–20] and quark [21–35] matter at different temperatures, while playing an important role in simulation of heavy-ion collisions [36–39]. For baryonic matter, the mean-field (MF)-based models rely on the phenomenological interactions whose parameters are fitted to the properties of the nuclear saturation point [40–49], while the microscopic ones employ the interactions extracted from nucleon–nucleon scattering data [50–58]. Within the MF approximation, the quark model of NJL can successfully illustrate different aspects of quantum chromo dynamics in both nonperturbative and perturbative regimes [59–68]. In this study, we focus on an isentropic analysis of a HHNS, utilizing a statistical MF model for baryonic matter, and the standard NJL model for quark matter to construct a hot hybrid EOS (HHEOS) via the Maxwell construction (adopted as a limiting case of the finite-size effects with large values of the baryon–quark surface tension). Incorporating the rearrangement effects by using the phase-space nucleon–nucleon interaction of Myers and Swiatecki (MS) [41, 69, 70], which is a density-dependent inverse-momentum extension of the basic interaction given by Seyler and Blanchard [42, 71–73], we determine the finite-temperature EOS of baryonic matter, based on a statistical approach that complies with the Thomas–Fermi approximation. This baryonic formalism has shown its efficiency in studying various thermodynamic aspects of nuclear matter [49, 74, 75], modeling a cold (hot) NS [76, 77] ([78–80]), and investigating the baryon–quark PT in a cold hybrid NS (CHNS) within the standard (local) NJL EOS of quark matter [63, 64, 68] and its non-local extension [67]. Thus, such theoretical attempts can be developed to probe the structure and composition of a HHNS. According to the comments mentioned above, we organize this manuscript as follows: In Sec. 2, we present our statistical MF model for baryonic matter, and the finite-temperature EOS of the deconfined quark phase within the standard NJL model. Sec. 3 is devoted to the discussion of our results obtained for HHNS matter in an isentropic picture with the help of the MC construction. Finally, the summary and conclusions are given in Sec. 4.

[a] e-mail: ghazanfari@kashanu.ac.ir (corresponding author)

Published online: 02 November 2023

2 Formalism

In this section, we present the EOS of baryonic matter, using a statistical approach based on the TF approximation, in which the state of each nucleon is determined by its momentum and position in the phase space. Moreover, the baryon–quark PT is illustrated with the help of the MC by introducing the quark matter EOS of the standard NJL at finite temperatures.

2.1 Baryonic mode

By assuming that nucleons are in β-equilibrium with relativistic electrons and muons, our Yukawa-type nucleon–nucleon interaction, given by Myers and Swiatecki [41, 69, 70], can be written as

$$V_{12} = -2T_b\rho_0^{-1} g\Big(\frac{r_{12}}{a}\Big)\Bigg\{\frac{1}{2}(1\mp\xi)\alpha - \frac{1}{2}(1\mp\zeta)\Bigg[\beta\Big(\frac{p_{12}}{p_b}\Big)^2 - \gamma\Big(\frac{p_b}{|p_{12}|}\Big) + \sigma\Big(\frac{2\bar{\rho}}{\rho_0}\Big)^{\frac{2}{3}}\Bigg]\Bigg\}, \tag{1}$$

where g is assumed to be a Yukawa-type function in terms of the relative distance r_{12} for each pair of nucleons, and the mean density $\bar{\rho}$ is expressed as a function of the nucleon density at the corresponding position of the two-body nucleon–nucleon interactions in phase space:

$$g\Big(\frac{r_{12}}{a}\Big) = \frac{1}{4\pi a^3}\frac{\exp\big(-\frac{r_{12}}{a}\big)}{\frac{r_{12}}{a}}, \quad \bar{\rho}^{\frac{2}{3}} = \frac{1}{2}\Big(\rho_1^{\frac{2}{3}} + \rho_2^{\frac{2}{3}}\Big). \tag{2}$$

Meanwhile, p_{12} is taken to be the relative momentum of the interacting particles. The adjustable parameters (a, α, β, γ, σ, ξ, ζ) are fitted to the saturation properties of normal nuclear matter and the coefficients of the Weizsacher–Bethe semiempirical mass formula as follows [69]:

$$\begin{aligned} a = 0.59294\,\text{fm}, \quad \alpha = 1.94684, \beta = 0.15311, \quad \gamma = 1.13672, \\ \sigma = 1.05, \quad \xi = 0.27976, \quad \zeta = 0.55665. \end{aligned} \tag{3}$$

In this interaction, the normal nuclear matter radius $r_0 = 1.14\,\text{fm}$ generates the saturation density $\rho_0 = (\frac{4}{3}\pi r_0^3)^{-1}$, the Fermi momentum $p_b = \hbar(\frac{3}{2}\rho_b\pi^2)^{\frac{1}{3}}$, and the associated kinetic energy $T_b = \frac{p_b^2}{2\bar{m}}$ with $\bar{m} = \frac{1}{2}\big(m_n + m_p\big) = 938.903\,\text{MeV/c}^2$ being the average nucleonic mass. According to this statistical model, the total nucleonic energy is given by

$$E_{MS} = \sum_{b=n,p}\frac{2}{h^3}\int d^3r_1\int d^3p_1\Big(\frac{p_1^2}{2m_b} + \frac{1}{2}V_b(p_1) + m_bc^2\Big)n_b(p_1), \tag{4}$$

where

$$V_{b=n,p}(p_1) = V_b^b(p_1) + V_b^{b'\neq b}(p_1), \tag{5}$$

with

$$V_b^b(p_1) = -\frac{4T_b}{\rho_0h^3}\Bigg\{\int d^3p_2n_b(p_2)\Bigg[\alpha_l - \beta_l\Big(\frac{p_{12}}{p_b}\Big)^2 + \gamma_l\frac{p_b}{|p_{12}|} - \sigma_l\Big(\frac{2\bar{\rho}}{\rho_0}\Big)^{\frac{2}{3}}\Bigg]\Bigg\}, \tag{6}$$

$$V_b^{b'}(p_1) = -\frac{4T_b}{\rho_0h^3}\Bigg\{\int d^3p_2n_{b'}(p_2)\Bigg[\alpha_u - \beta_u\Big(\frac{p_{12}}{p_b}\Big)^2 + \gamma_u\frac{p_b}{|p_{12}|} - \sigma_u\Big(\frac{2\bar{\rho}}{\rho_0}\Big)^{\frac{2}{3}}\Bigg]\Bigg\}, \tag{7}$$

by using the upper (lower) signs for the interaction between like (unlike) particles as

$$\begin{aligned} \alpha_{l,u} = \frac{1}{2}(1\mp\xi)\alpha, \quad \beta_{l,u} = \frac{1}{2}(1\mp\zeta)\beta, \\ \gamma_{l,u} = \frac{1}{2}(1\mp\zeta)\gamma, \quad \sigma_{l,u} = \frac{1}{2}(1\mp\zeta)\sigma. \end{aligned} \tag{8}$$

For the phase-space occupation number $n_b(p_)$ of the bth nucleon, which minimizes the total thermodynamic potential $\Omega_{\text{MS}} = E_{MS} - T\sum_{b=n,\,p}S_b - \sum_{b=n,\,p}\mu_bN_b$ (with S_b and N_b being the associated entropy and particle number) at given temperature T and chemical potential μ_b, we have [75]:

$$n_b(p_) = \frac{1}{1 + \exp[(h_b(p_) - \mu_b)/T]}. \tag{9}$$

The phase-space single-particle energy $h_b(p) = \frac{p^2}{2B_b} + U_b(p) + \bar{m}c^2$ is expressed in terms of the effective mass

$$B_b = \frac{\bar{m}}{1 + \frac{2\rho_b}{\rho_0}\beta_l + \frac{2\rho_{b'}}{\rho_0}\beta_u}, \tag{10}$$

and the single-particle potential $U_b(p_)$. Finally, the nuclear EOS is obtained using the self-consistent relations between the density ρ_b and the single-particle potential $U_b(p_)$ as follows:

$$\rho_{\rm B} = \sum_{b=n,p} \frac{2}{h^3} \int d^3 p_1 n_b(p_1), \tag{11}$$

$$\begin{aligned} U_b(p) = &\left(-\frac{16\pi p_b T_b}{\rho_0 h^3}\right)\left\{\gamma_l\left(\frac{\psi_b^(p)}{p} + \phi_b(p)\right) + \gamma_u\left(\frac{\psi_{b'}^(p)}{p} + \phi_{b'}^(p)\right)\right\} \\ &+ \frac{2\,T_b}{\rho_0}\left\{-\alpha_l\rho_b - \alpha_u\rho_{b'} + \beta_l k_b + \beta_u k_{b'} + \frac{4}{3}\,\sigma_l\,\rho_b\left(\frac{2\,\rho_b}{\rho_0}\right)^{\frac{2}{3}}\right. \\ &\left. + \frac{5}{6}\sigma_u\,\frac{\rho_{b'}}{2}\,(\frac{2\,\rho_b}{\rho_0})^{\frac{2}{3}} + \frac{\sigma_u\rho_{b'}}{2}\left(\frac{2\rho}{\rho_0}\right)^{\frac{2}{3}}\right\} \end{aligned} \tag{12}$$

with

$$\begin{aligned} k_{b(b')} &= \frac{2}{h^3}\int\left(\frac{p_1}{p_b}\right)^2 n_{b(b')}(p_1)\,d^3p_1, \\ \psi_{b(b')}(p_1) &= \int_0^{p_1} p_2^2 n_{b(b')}(p_2)\,dp_2, \\ \phi_{b(b')}(p_1) &= \int_{p_1}^{\infty} p_2\,n_{b(b')}(p_2)\,dp_2. \end{aligned} \tag{13}$$

Employing the chemical potential of nucleons, and relativistic leptons including muons, electrons, and also trapped neutrinos, we can determine the properties of charge-neutral dense matter under the β-equilibrium conditions:

$$\mu_{n^0} - \mu_{p^+} = \mu_{e^-} - \mu_{\rm Le} = \mu_{\mu^-} - \mu_{L\mu}, \tag{14}$$

$$\rho_{p^+} = \rho_{e^-} + \rho_{\mu^-}. \tag{15}$$

In the above, the electron (muon) lepton number chemical potential $\mu_{Le(\mu)}$ distinguishes the neutrino-trapped case, where $\mu_{\rm Le} = \mu_{\nu_e^0}(-\mu_{\bar{\nu}_\mu^0})$, from the neutrino-free one with $\mu_{\rm Le} = 0$ ($\mu_{L\mu} = 0$). The energy density of β-stable nuclear matter $e = e_{MS} + e_L + e_\gamma$ includes the contributions from the nucleonic energy density $e_{MS} = E_{MS}/V$, the leptonic energy density $e_L = \sum_{l=e^-,\mu^-,\nu_e^0,\bar{\nu}_\mu^0} \frac{2}{h^3}\int d^3p\,E_p(p)\,n_l(p)$ (with $E_p(p) = \sqrt{(pc)^2 + (m_l c^2)^2}$ and $n_l(p) = \left(1 + \exp\left[\frac{(E_p(p)-\mu_l)}{T}\right]^{-1}\right)$), and the photon energy density $e_\gamma = \frac{\pi^2}{15}\frac{T^4}{(\hbar c)^3}$ obtained from the blackbody model [81–83]. Using the nucleonic and leptonic occupation numbers, one can determine the entropy density in the presence of photons as:

$$\begin{aligned} s = s_N + s_L + s_\gamma = \sum_{i=N,L}\frac{-2}{h^3}\Big\{\int d^3p_1\,[n_i(p_1)\ln(n_i(p_1)) \\ + (1 - n_i(p_1))\ln(1 - n_i(p_1))]\Big\} + \frac{4}{3}\,\frac{e_\gamma}{T}. \end{aligned} \tag{16}$$

For the EOS of dense matter, one needs the free energy density $f = e - Ts$ to calculate the pressure according to

$$P = \sum_{i=N,L}(\mu_i\rho_i) - f. \tag{17}$$

2.2 Standard NJL model

We adopt the standard three-flavor NJL model, based on the following Lagrangian to derive the EOS of quark matter at finite temperatures:

$$\begin{aligned} \mathcal{L}_{NJL} = &\bar{q}\left(i\gamma_\mu\partial^\mu - m^0\right)q + G_S\sum_{a=0}^{8}\left[(\bar{q}\lambda_a q)^2 + (\bar{q}\gamma_5\lambda_a q)^2\right] - K\left\{\det\left[\bar{q}(1+\gamma_5)q\right]\right. \\ &\left.+\det\left[\bar{q}(1-\gamma_5)q\right]\right\} - G_{\rm V}\sum_{a=0}^{8}\left[\left(\bar{q}\gamma_\mu\lambda_a q\right)^2 + \left(\bar{q}\gamma_5\gamma_\mu\lambda_a q\right)^2\right]. \end{aligned} \tag{18}$$

In the above relation, q is the quark field, $m^0 = {\rm diag}\left(m_{d^-}^0, m_{u^+}^0, m_{s^-}^0\right)$ denotes the current quark mass matrix, and the Gell-Mann matrices $\lambda_a\,(a = 1, 2, ..., 8)$ in the color space are accompanied by $\lambda_0 = \sqrt{\frac{2}{3}}\infty_{3\times3}$. Here, G_s, K, and $G_{\rm V}$ are the coupling

constants of the scalar Kobayashi-Maskawa-'t Hooft, and vector interactions, respectively. Based on the MF approximation, the NJL thermodynamic potential density Ω_{NJL}, in which the regularization scheme is given by the ultraviolet cutoff parameter Λ, can be written as

$$\Omega_{NJL} = -\sum_{q=u,d,s}\frac{3}{\pi^2}\int_0^{\Lambda} dpp^2\Big[E_p^{(M_q)} + T\ln\Big(1+\exp\Big[-\Big(E_p^{(M_q)}-\tilde{\mu}_q\Big)/T\Big]\Big)$$
$$T\ln\Big(1+\exp\Big[-\Big(E_p^{(M_q)}+\tilde{\mu}_q\Big)/T\Big]\Big)\Big] - 4K\langle\bar{q}_u q_u\rangle\langle\bar{q}_d q_d\rangle\langle\bar{q}_s q_s\rangle$$
$$+\sum_{q=u,d,s}2G_S\langle\bar{q}_q q_q\rangle^2 - \sum_{q=u,d,s}2G_{\rm V}\langle q_q^{\dagger}q_q\rangle^2;\quad E_p^{(M_q)} = \sqrt{M_q^2+p^2}, \tag{19}$$

where the renormalized quark chemical potential $\tilde{\mu}_q$, and the dynamically generated quark mass M_q are found to be

$$\tilde{\mu}_q = \mu_q - 4G_{\rm V}\langle q_q^{\dagger}q_q\rangle, \tag{20}$$

$$M_q = m_q - 4G_S\langle\bar{q}_q q_q\rangle + 2K\langle\bar{q}_{q'}q_{q'}\rangle\langle\bar{q}_{q''}q_{q''}\rangle. \tag{21}$$

In the so-called gap equation Eq. (21), $(q,\ q',\ q'')$ stands for any permutation of $(u,\ d,\ s)$ quarks. Pursuing the MF constraints $\frac{\partial\Omega_{NJL}}{\partial M_q} = \frac{\partial\Omega_{NJL}}{\partial\tilde{\mu}_q} = 0$, one can reach the following relations for the qth quark condensate $\langle\bar{q}_q q_q\rangle$ and, qth quark number density $\langle q_q^{\dagger}q_q\rangle$

$$\langle\bar{q}_q q_q\rangle = -\frac{3}{\pi^2}\int_0^{\Lambda} dpp^2\frac{M_q}{E_p^{(M_q)}}\big[1-n_q-\bar{n}_q\big], \tag{22}$$

$$\langle q_q^{\dagger}q_q\rangle = \rho_q = \frac{3}{\pi^2}\int_0^{\Lambda} dpp^2\big[n_q-\bar{n}_q\big], \tag{23}$$

with

$$n_q = \frac{1}{\exp\big[\big(E_p-\tilde{\mu}_q\big)/T\big]+1}, \tag{24}$$

$$\bar{n}_q = \frac{1}{\exp\big[\big(E_p+\tilde{\mu}_q\big)/T\big]+1}. \tag{25}$$

For a neutral mixture of quarks and leptons, the β-equilibrium conditions can be read in terms of the baryonic chemical potential $\mu_{\rm B} = \frac{2\mu_{d^-}+\mu_{u^+}}{3} \equiv \frac{\mu_{n^0}}{3}$ as

$$\mu_{u^+} = \mu_{\rm B} - \frac{2}{3}(\mu_{e^-}-\mu_{\rm Le}), \tag{26}$$

$$\mu_{d^-} = \mu_{s^-} = \mu_{\rm B} + \frac{1}{3}(\mu_{e^-}-\mu_{\rm Le}), \tag{27}$$

$$\mu_{e^-} - \mu_{\rm Le} = \mu_{\mu^-} - \mu_{L\mu}, \tag{28}$$

$$\frac{2}{3}\rho_{u^+} - \frac{1}{3}(\rho_{d^-}+\rho_{s^-}) - \big(\rho_{e^-}+\rho_{\mu^-}\big) = 0. \tag{29}$$

In this work, we use the interaction parameters of the RKH set [60] m_{u^+}=$m_{d^-} = 5.5\,\text{MeV}$,$m_{s^-} = 140.7\,\text{MeV}$, $\Lambda = 602.3\,\text{MeV}$, $G_s = \frac{1.835}{\Lambda^2}$, $K = \frac{12.36}{\Lambda^5}$ to perform the self-consistent calculations by considering the vector strength ratio $\eta_{\rm V} = G_{\rm V}/G_S$, adopted as a free parameter because of the theoretical uncertainty. Despite lacking a stringent constraint on $\eta_{\rm V}$, its value, which has a strong impact on determining the critical point for the chiral phase transition, is estimated to lie in the range 0–1.1, as suggested by most studies, including those on relativistic heavy ion collisions [84–87]. Consequently, the pressure of quark matter in β-equilibrium is calculated by

$$P = P_{NJL} + P_L + P_\gamma, \tag{30}$$

with

$$P_{NJL} = \Omega_{NJL}^0 - \Omega_{NJL}, \tag{31}$$

$$P_L = \sum_{l=e^-,\mu^-,\nu_e^0,\bar{\nu}_\mu^0}(\mu_l\rho_l) - e_L + Ts_L, \tag{32}$$

$$P_\gamma = \frac{e_\gamma}{3}. \tag{33}$$

In Eq. (31), Ω^0_{NJL} ensures zero pressure in the vacuum. In addition, one can determine the free energy density f, and energy density e by

$$f = \sum_{k=Q,L} (\mu_k \rho_k) - P, \tag{34}$$

$$e = Ts + f, \tag{35}$$

with the entropy density of β-stable quark matter s, given by

$$s = \sum_{q=u^+,d^-,s^-} \frac{-6}{h^3} \left\{ \int d^3 p_1 \left[n_q(p_1) \ln(n_q(p_1)) + (1 - n_q(p_1)) \ln(1 - n_q(p_1)) \right] \right\} + s_L + s_\gamma. \tag{36}$$

3 Results and discussion

This work aims to clarify the thermal effects on the baryon–quark PT in an isentropic analysis signified by the entropy per baryon $S = \frac{s}{\rho_B}$, according to the MC. We have employed the statistical approach, using the MS interaction for baryons, and the standard NJL model for the deconfined quark phase to model the structure of HHNSs with β-equilibrated dense matter in the presence (absence) of trapped neutrinos. When the finite-size effects are taken into account for a given temperature, the mixed-phase scenario approaches the MC at sufficiently large values of the baryon–quark surface tension, which means both phases become close to being separately charge-neutral with equal pressure and baryonic chemical potential, and therefore, a jump is induced in the thermodynamic quantities. However, simulating HHNSs in an isentropic picture demands determining the thermodynamic quantities in the coexistence region even if the MC is adopted [12]. Therefore, one can employ the baryonic volume fraction χ to linearly interpolate the mixed-phase data at the constant entropy per baryon S in terms of the baryonic density ρ_B, according to

$$\chi s^{(BP)} + (1 - \chi) s^{(QP)} = \rho_B S, \tag{37}$$

$$\chi \rho_B^{(BP)} + (1 - \chi) \rho_B^{(QP)} = \rho_B. \tag{38}$$

Just after the core bounce of a proto-NS, which is a hot and lepton-rich newborn NS as a result of a supernova explosion, one can assume the electron lepton number $Y_{Le} = \frac{\rho_{e^-} + \rho_{\nu_e 0}}{\rho_B}$ is constant with the typical value $Y_{Le} \sim 0.4$ [1, 2] across the stellar core, while the electron lepton number $Y_{L\mu} = \frac{\rho_{\mu^-} - \rho_{\bar{\nu}_\mu 0}}{\rho_B}$ vanishes. The diffusion of trapped neutrinos, taking place outwards from the stellar core, gives rise to the deleponization (heating) stage, characterized simultaneously by increasing the entropy per baryon, and decreasing the lepton electron number. In this study, the core at the start (end) of this stage is considered to be made of neutrino-trapped (neutrino-transparent) matter with $Y_{Le} = 0.4$ and $S = 1$ ($\mu_{Le} = 0$ and $S = 2$).

Studying the PT from baryons to quarks requires extracting the EOS of each pure phase. For the occurrence of the baryon–quark PT at a given temperature, the baryon and quark EOSs must intersect each other in the pressure-baryon chemical potential ($P - \mu_B$) plane. For this reason, P as a function of μ_B is shown in Fig. 1 for the neutrino-trapped matter and neutrino-free matter at various temperatures. It is shown that all cases of neutrino-trapped (neutrino-free) matter lead to the baryon–quark PT. With increasing T, there is a tendency for the PT to occur at lower values of P and μ_B, while with rising the vector coupling strength η_V, the PT is shifted to higher values of these quantities. In general, the PT is described in the neutrino-trapped case with smaller amounts of P and μ_B.

In contrast to an isothermal PT under the MC, the baryonic chemical potential μ_B and pressure P are not taken to be constant in the mixed-phase region for an isentropic Maxwell-like PT. Figures 2 and 3 shows the isentropic behavior of μ_B (P) as an increasing

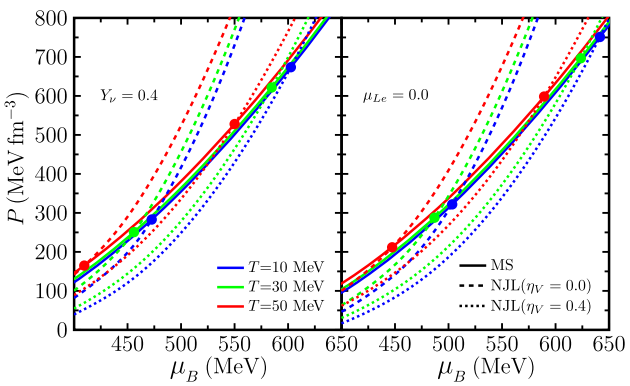

Fig. 1 Pressure as a function of baryonic chemical potential for neutrino-trapped matter (left panel) and neutrino-free matter (right panel) at the temperatures $T = 10$, 30 and 50 MeV, employing the MS baryonic interaction and the NJL quark model with the vector strength ratios $\eta_V = 0$, 0.4. The crossing points of the baryonic and quark EOSs denote the baryon–quark PT under the MC

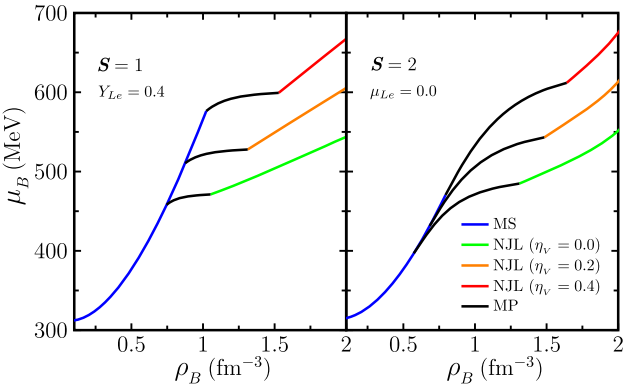

Fig. 2 Baryonic chemical potential as a function of baryonic density for neutrino-trapped matter (left panel) and neutrino-free matter (right panel), utilizing the MS baryonic interaction and the NJL quark model with the vector strength ratios $\eta_V = 0$, 0.02, 0.4. The mixed-phase regions are denoted by MP

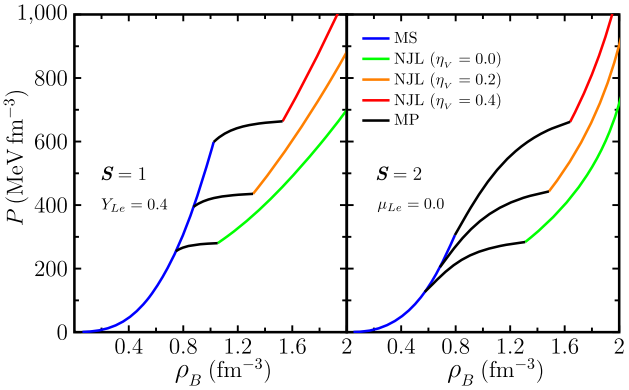

Fig. 3 Pressure as a function of baryonic density for neutrino-trapped matter (left panel) and neutrino-free matter (right panel), using the MS baryonic interaction and the NJL quark model with the vector strength ratios $\eta_V = 0$, 0.02, 0.4. The mixed-phase regions are denoted by MP

function of baryonic density. As seen in this figure, the mixed-phase EOS for neutrino-trapped matter is significantly softer than the one for neutrino-free matter. It should be noted that increasing η_V changes dramatically the mixed-phase characteristics, pushing the onset of the PT to higher baryonic densities, and enlarging the width of the mixed phase. Compared with neutrino-trapped matter, the width of the coexistence region is larger for neutrino-free matter, and the PT emerges at lower baryonic densities.

In order to understand the composition of HHNSs, the number fraction of bth baryon (lth lepton) $\frac{\rho_{b(l)}}{\rho_B}$ and qth quark $\frac{\rho_q}{3\rho_B}$ are presented in Figs. 4 and 5 for neutrino-trapped matter and neutrino-free matter, respectively. In the pure baryonic phase, the neutrons constitute the most abundant particles, and their relative fraction remains nearly constant with increasing baryonic density. The quark degrees of freedom, which grow dramatically in the mixed-phase region, give rise to a considerable decrease of the electron and muon abundances due to the charge neutrality condition, as this influence is observed more considerably in neutrino-trapped matter than in neutrino-free matter. In neutrino-trapped matter for each η_V value, the muon anti-neutrino abundance, especially at higher baryonic densities, turns out to be almost negligible because of the constraint $Y_{L\mu} = 0$, while the electron neutrino abundance (besides the meaningful contribution of electrons) is large enough so that it becomes comparable with the quark fractions at high baryonic densities. Unlike neutrino-trapped matter, muons are taken into in the composition of neutrino-transparent matter at the whole baryonic density range.

The adiabatic sound speed has particular significance in checking the causality condition and hydrodynamic stability for dense stellar matter. We display in Fig. 6 the squared ratio of sound speed to the light speed $(v_s/c)^2 = (\partial P/\partial e)_S$ against baryonic density, as it is less than one for all of the HHEOSs. Unlike the pure baryon and quark phases, the mixed-phase region indicates that the sound speed is a decreasing function of baryonic density. With an increase in η_V of each HHEOS, the sound speed reaches larger values, especially in the pure baryon (quark) phase of neutrino-trapped (neutrino-free) matter. In addition, the sensitivity of the sound speed to η_V becomes weaker for neutrino-free matter, as the baryonic density increases in the pure quark phase region.

The adiabatic index $\Gamma_S = \frac{e}{P}(\frac{v_s}{c})^2$, which can characterize an isentropic EOS as $P \propto e^{\Gamma_S}$ to give a measure of its stiffness, is shown in Fig. 7 as a function of baryonic density for all of the HHEOSs. It can be seen that the larger Γ_S values are calculated in the pure quark region of neutrino-free matter, while the lower ones belong to the mixed-phase region of neutrino-trapped matter. In addition, increasing η_V cannot significantly alter the adiabatic index range.

In this isentropic picture of HHNS matter, it is crucial to clarify the behavior of temperature as a function of baryonic density (see Fig. 8). According to this figure, neutrino-trapped matter shows a slower change of the temperature with the baryonic density than neutrino-free matter. As can be found, the outcome of rising the pressure with the baryonic density in the mixed-phase region is dropping the temperature, since one can conclude from Fig. 1 that decreasing the temperature leads to increasing the mixed-phase pressure, i.e., $\left(\frac{\partial P}{\partial T}\right)_{\rm MP} < 0$. As a consequence, the temperature reaches its maximum value at the threshold baryonic density for

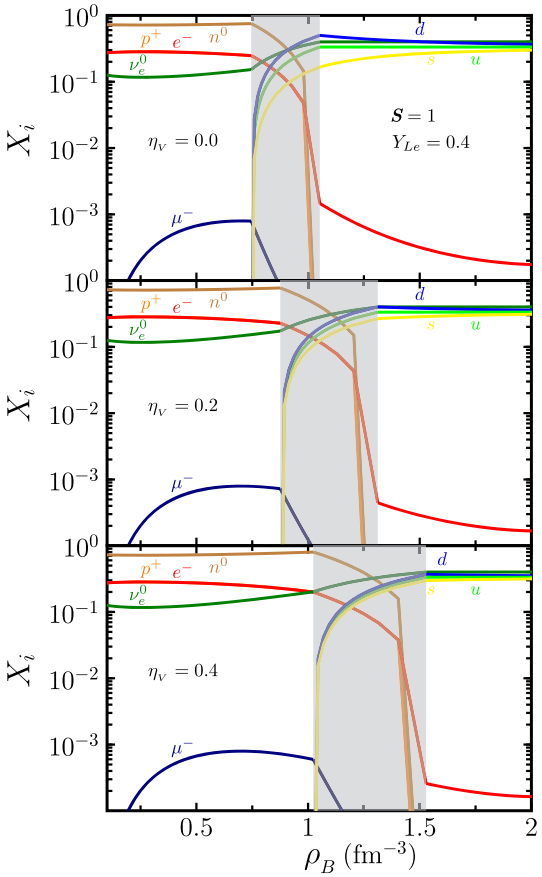

Fig. 4 Number fraction of leptons, baryons, and quarks as a function of baryonic density for neutrino-trapped matter, utilizing the MS baryonic interaction and the NJL quark model with the vector strength ratios $\eta_V = 0$, 0.02, 0.4. The shaded areas indicate the mixed-phase regions

the PT onset. It should be mentioned that the temperature in the pure quark region demonstrates a weak dependence on the vector coupling ratio η_V.

The global structure of HHNS can be studied using the well-known hydrostatic equilibrium equations of Tolman–Oppenheimer–Volkoff (TOV) [88, 89], given by

$$\frac{\mathrm{d}P(r)}{\mathrm{d}r} = -\frac{m_G(r)e(r)}{r^2}\frac{\left[1+\frac{P(r)}{e(r)}\right]\left[1+\frac{4\pi r^3 P(r)}{m_G(r)}\right]}{1-\frac{2m_G(r)}{r}}, \tag{39}$$

$$\frac{\mathrm{d}m_G(r)}{\mathrm{d}r} = 4\pi r^2 e(r), \tag{40}$$

with P, e, m_G being the pressure, energy density, and enclosed gravitational mass at the distance r from the star center. In addition, one can employ simultaneously the TOV equations with the following relation to calculate the baryonic mass of a HHNS:

$$\frac{\mathrm{d}m_B(r)}{\mathrm{d}r} = 4\pi r^2 \frac{\rho_B \bar{m}}{\sqrt{1-\frac{2m_G(r)}{r}}}. \tag{41}$$

Our HHEOSs, which constitute the basic inputs for Eqs. (39)–(41), are joined to the EOS of a cold solid crust given in Ref. [90] ([91]) for the inner (outer) crust. The output results for the gravitational and baryonic masses vs. the central baryonic density are displayed in Fig. 9. It can be seen that the baryonic mass is always greater than the gravitational mass. The gravitational (baryonic) mass of each case of HHNS matter is specified by a maximum value, which becomes larger as η_V increases. These maximum masses are slightly affected by neutrino trapping. Moreover, a HHNS can be formed with higher values of the central baryonic density in neutrino-trapped matter than in neutrino-free matter.

In Fig. 10, we show a roughly linear relation between the gravitational and baryonic masses. The acceptable ranges for a stable mass structure of a HHNS can be understood via the maximum baryonic mass of a CHNS since the baryonic mass must be conserved in the cooling process of a new-born NS. As a result, the mass structures for each η_V are found to be stable up to the maximum mass structure because of not exceeding the baryonic mass of a CHNS, while adopting the pure baryonic EOS of MS as an input in the TOV equations can lead to the unstable structures for neutrino-free matter (see Ref. [80]).

Our results for the mass-radius relation of a HHNS, compared with those obtained for a CHNS, are depicted in Fig. 11. In addition to the larger values of the gravitational mass, smaller radii are allowed with strengthening the quark vector interaction. Within our

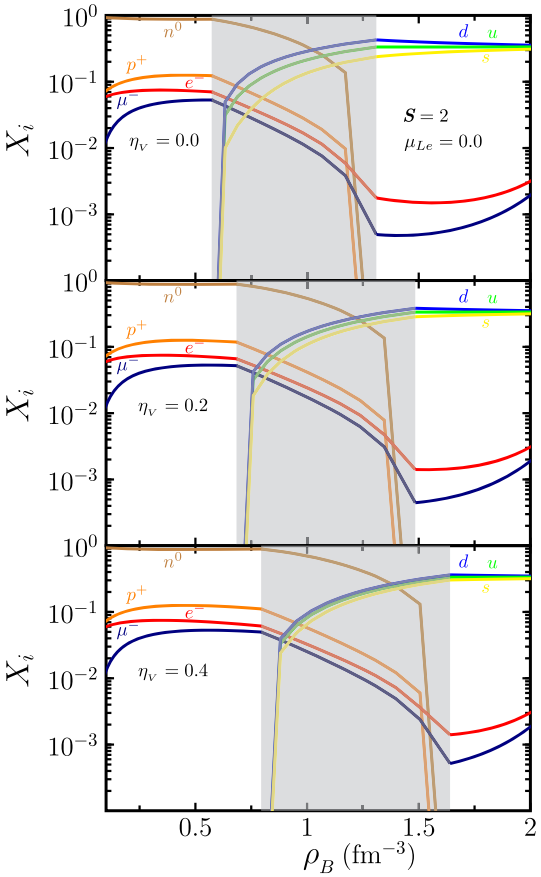

Fig. 5 Same as Fig. 4 but for neutrino-free matter

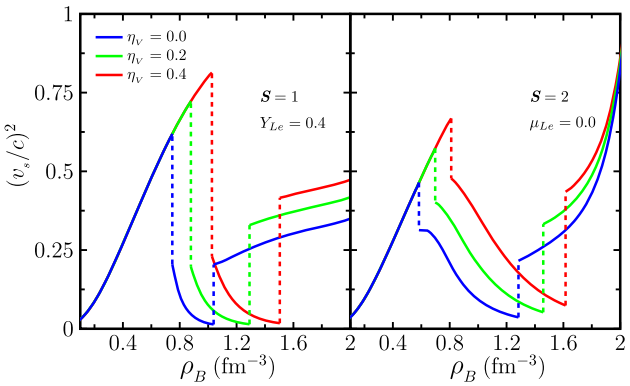

Fig. 6 Squared speed of sound (in units of the speed of light) as a function of baryonic density for neutrino-trapped matter (left panel) and neutrino-free matter (right panel), employing the MS baryonic interaction and the NJL quark model with the vector strength ratios $\eta_V = 0$, 0.02, 0.4

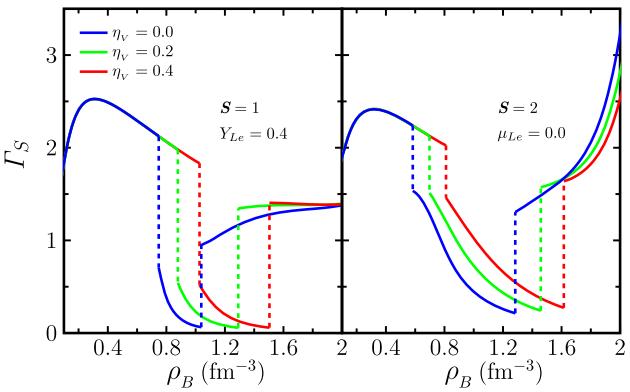

Fig. 7 Adiabatic index as a function of baryonic density for neutrino-trapped matter (left panel) and neutrino-free matter (right panel), using the MS baryonic interaction and the NJL quark model with the vector strength ratios $\eta_V = 0$, 0.02, 0.4

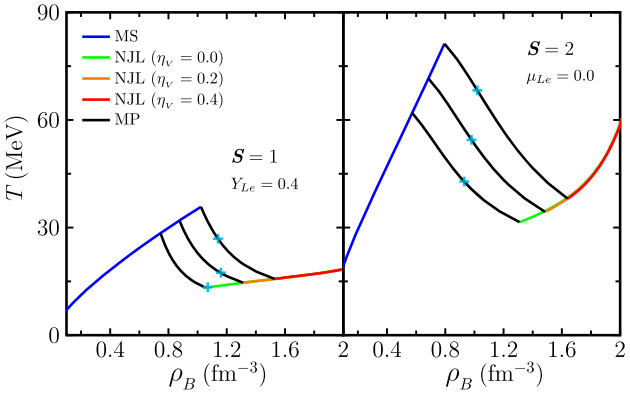

Fig. 8 Temperature as a function of baryonic density for neutrino-trapped matter (left panel) and neutrino-free matter (right panel), using the MS baryonic interaction and the NJL quark model with the vector strength ratios $\eta_V = 0$, 0.02, 0.4. The mixed-phase regions are denoted by MP. The plus signs indicate the central temperature and density of a HHNS at the maximum mass configuration

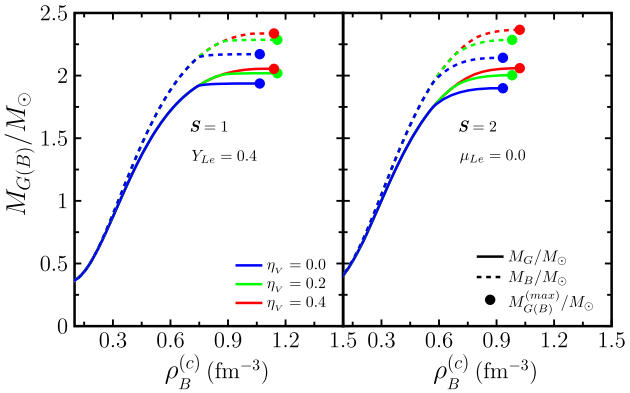

Fig. 9 Gravitational (baryonic) mass (in units of the solar mass $M_\odot$) as a function of central baryonic density for neutrino-trapped matter (left panel) and neutrino-free matter (right panel), utilizing the MS baryonic interaction and the NJL quark model with the vector strength ratios $\eta_V = 0$, 0.02, 0.4. The maximum masses are denoted by the filled circles

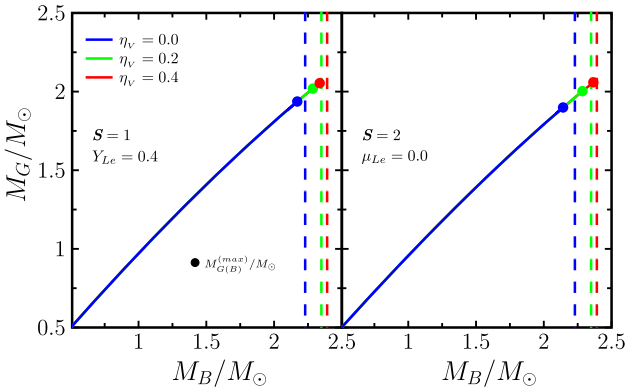

Fig. 10 Gravitational mass (in units of the solar mass $M_\odot$) as a function of baryonic mass (in units of the solar mass $M_\odot$) for neutrino-trapped matter (left panel) and neutrino-free matter (right panel), utilizing the MS baryonic interaction and the NJL quark model with the vector strength ratios $\eta_V = 0$, 0.2, 0.4. The filled circles denote the maximum mass structures, and the dashed vertical lines indicate the maximum baryonic mass of a CHNS, corresponding to $M_B = 2.23$, 2.35, 2.39 $M_\odot$ for the quark vector strength ratios $\eta_V = 0$, 0.02, 0.4, respectively

isentropic study, a HHNS can be described by the slightly smaller radii as a result of neutrino trapping. According to the present approach, the gravitational constraints J0740+6620 and J0030 + 0451 are also fulfilled for a CHNS, which can be predicted by the smaller radii. For the sake of completeness, Table 1 demonstrates the maximum mass properties of a HHNS for all HHOSs, as the maximum gravitational masses are in the range 1.94−2.05 $M_\odot$ (1.90−2.06 $M_\odot$) for neutrino-trapped (neutrino-free) matter. As also indicated in Fig. 8, the neutrino trapping can lead to the appearance of the pure quark phase in the stellar core, when the vector coupling ratio η_V approaches zero.

4 Summary and conclusion

In this work, we have paid the main attention to an isentropic analysis of thermal effects on the baryon–quark PT in neutrino-trapped (neutrino-transparent) β-stable matter within the MC, adopting a statistical MF model which is consistent with the TF approximation for the baryonic EOS, and the standard NJL model for the deconfined quark phase to model the structure and composition of a HHNS. According to our results, the pressure and baryonic chemical potential are increasing functions of the density in the mixed-phase

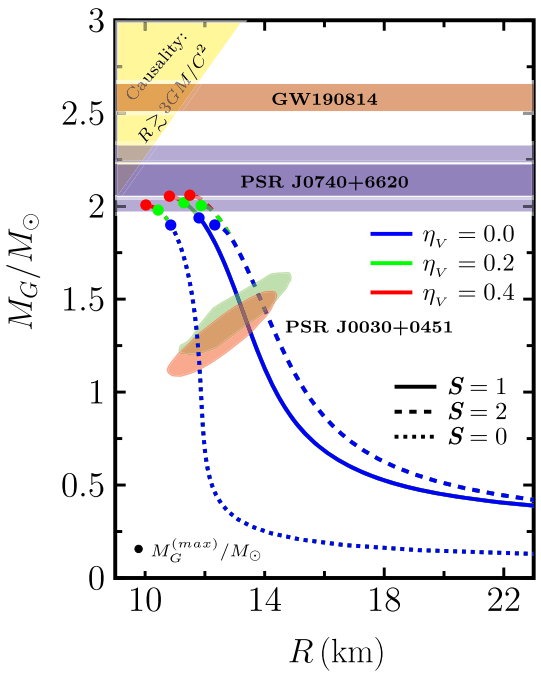

Fig. 11 Mass-radius diagrams of neutrino-trapped matter at $S = 1$, and neutrino-free matter at $S = 2$ for a HHNS and $S = 0$ for a CHNS, utilizing the MS baryonic interaction and the NJL quark model with the vector strength ratios $\eta_V = 0$, 0.02, 0.4. The filled circles denote the maximum mass structures. The observational mass constraint from PSR J0740+6620 [92], the gravitational mass inferred for the light component of [93], and the area of the mass-radius limits deduced from the NICER measurements of PSR J0030+0451 [94, 95] are displayed, while the region on the top-left of this figure is excluded by causality [96]

Table 1 Characteristics of a HHNS at the maximum mass configuration for the EOS of neutrino-trapped matter (the cases with $S = 1$) and neutrino-free matter (the cases with $S = 2$), given by the mixed-phase baryonic density range $\rho_B^{(MP)}$, in terms of the central baryonic density $\rho_B^{(c)}$, the central energy density $e^{(c)}$, the central pressure $P^{(c)}$, the gravitational (baryonic) mass M_G (M_B) (in units of the solar mass $M_\odot$), the stellar radius R, and the central temperature T_c, employing the MS baryonic interaction and the NJL quark model with the vector strength ratios $\eta_V = 0$, 0.02, 0.4

	$\rho_B^{(MP)}$ (fm^{-3})	$\rho_B^{(c)}$ (fm^{-3})	$e^{(c)}$ ($\mathrm{MeV\,fm}^{-3}$)	$P^{(c)}$ ($\mathrm{MeV\,fm}^{-3}$)	M_G ($M_\odot$)	M_B ($M_\odot$)	R (km)	T_c (MeV)
$S = 1$								
$\eta_V = \mathbf{0.0}$	**0.75−1.05**	**1.07**	**1323.94**	**283.97**	**1.94**	**2.17**	**11.80**	**13.35**
$\eta_V = 0.2$	0.88-1.31	1.16	1524.90	430.79	2.02	2.29	11.29	17.40
$\eta_V = 0.4$	1.02-1.53	1.14	1553.60	632.70	2.05	2.34	10.81	26.89
$S = 2$								
$\eta_V = 0.0$	0.57-1.31	0.93	1137.35	246.64	1.90	2.14	12.33	42.84
$\eta_V = 0.2$	0.68-1.48	0.98	1237.82	350.37	2.00	2.29	11.88	54.46
$\eta_V = 0.4$	0.79-1.64	1.02	1323.94	464.37	2.06	2.37	11.50	68.25

The bold data indicate the emergence of a pure quark phase in the stellar core under the MC

zone, while the temperature shows a decreasing behavior. Meanwhile, trapped neutrinos make the mixed-phase EOS significantly softer than free-streaming neutrinos do. Stiffening the HHEOS by strengthening the quark vector interaction has a strong effect on the characteristics of the coexistence phase, delaying the onset of the PT to higher baryonic densities, and broadening the density range of the mixed phase. We have also checked the causality condition in hot dense stellar matter by calculating the sound velocity in units of the light velocity, which is always less than one for all of our HHEOSs. For each HHEOS, the temperature reaches its maximum value at the threshold baryonic density for the PT onset. Moreover, the temperature demonstrates a weak dependence on the vector coupling ratio η_V in the pure quark region. For the neutrino-trapped case, the pure quark phase can be allowed to occur in the core of a HHNS, as the vector coupling ratio η_V is varied toward zero. The predicted mass structures for a HHNS are found to be gravitationally stable because the maximum baryonic masses cannot exceed the maximum baryonic mass of a CHNS.

Acknowledgements Authors would like to thank University of Kashan for supporting this project under the Grant Number 1222393/1 provided by the Research Council.

Data Availability Statement This manuscript has no associated data or the data will not be deposited.

References

1. M. Prakash, I. Bombaci, M. Prakash, P.J. Ellis, J.M. Lattimer, R. Knorren, Phys. Rep. **280**, 1 (1997)
2. J.A. Pons, S. Reddy, M. Prakash, J.M. Lattimer, J.A. Miralles, Astrophys. J. **513**, 780 (1999)
3. H. Shen, H. Toki, K. Oyamatsu, K. Sumiyoshi, Astrophys. J. **197**, 20 (2011)
4. K. Sumiyoshi, S. Furusawa, H. Nagakura, A. Harada, H. Togashi, K. Nakazato, H. Suzuki, Prog. Theor. Exp. Phys. **2023**, 013E02 (2023)
5. D.P. Menezes, C. Providência, Phys. Rev. C **69**, 045801 (2004)
6. G.F. Burgio, S. Plumari, Phys. Rev. D **77**, 085022 (2008)
7. I. Bombaci, D. Logoteta, C. Providência, I. Vidana, Astron. Astrophys. **528**, A71 (2011)
8. H. Chen, M. Baldo, G.F. Burgio, H.-J. Schulze, Phys. Rev. D **86**, 045006 (2012)
9. H. Chen, G.F. Burgio, H.-J. Schulze, N. Yasutake, Astron. Astrophys. **551**, A13 (2013)
10. M. Hempel, O. Heinimann, A. Yudin, I. Iosilevskiy, M. Liebendörfer, F.K. Thielemann, Phys. Rev. D **94**, 103001 (2016)
11. M. Mariani, M. Orsaria, H. Vucetich, Astron. Astrophys. **601**, A21 (2017)
12. T. Fischera, Eur. Phys. J. A **57**, 270 (2021)
13. D. Logoteta, I. Bombaci, A. Perego, Eur. Phys. J. A **58**, 55 (2022)
14. O. Ivanytskyi, D. Blaschke, Eur. Phys. J. A **58**, 152 (2022)
15. A. Sedrakian, A. Harutyunyan, Universe **7**, 382 (2021)
16. X. Viñas Gausí, C. González Boquera, M. Centelles Aixalà, C. Mondal, L.M. Robledo. Symmetry (2021)
17. G. Grams, J. Margueron, R. Somasundaram, S. Reddy, Eur. Phys. J. A **58**, 56 (2022)
18. H. Tong, C. Wang, S. Wang, Astrophys. J. **930**, 137 (2022)
19. Z. Zhu, A. Li, T. Liu, Astrophys. J. **943**, 163 (2023)
20. J.M. Lattimer, Particles **6**, 30 (2023)
21. T. Klähn, D. Blaschke, F. Sandin, C. Fuchs, A. Faessler, H. Grigorian, G. Röpke, J. Trümper, Phys. Lett. B **654**, 170 (2007)
22. F. Yang, H. Shen, Phys. Rev. C **77**, 025801 (2008)
23. N. Yasutake, K. Kashiwa, Phys. Rev. D **79**, 043012 (2009)
24. H. Chen, M. Baldo, G.F. Burgio, H.J. Schulze, Phys. Rev. D **84**, 105023 (2011)
25. P.C. Chu, X.H. Li, B. Wang, Y.M. Dong, Y.Y. Jia, S.M. Wang, H.Y. Ma, Eur. Phys. J. C **77**, 512 (2017)
26. C.J. Xia, T. Maruyama, N. Yasutake, T. Tatsumi, H. Shen, H. Togashi, Phys. Rev. D **102**, 023031 (2020)
27. M. Kumari, A. Kumar, Eur. Phys. J. C **81**, 791 (2021)
28. I.A. Rather, A.A. Usmani, S.K. Patra, J. Phys. G **48**, 085201 (2021)
29. K. Huang, J. Hu, Y. Zhang, H. Shen, Astrophys. J. **935**, 88 (2022)
30. G.A. Contrera, D. Blaschke, J.P. Carlomagno, A.G. Grunfeld, S. Liebing, Phys. Rev. C **105**, 045808 (2022)
31. S. Pal, S. Podder, D. Sen, G. Chaudhuri, Phys. Rev. D **107**, 063019 (2023)
32. C.H. Lenzi, M. Dutra, O. Lourenço, L.L. Lopes, D. Menezes, Eur. Phys. J. C **83**, 266 (2023)
33. A. Kumar, V.B. Thapa, M. Sinha, Phys. Rev. D **107**, 063024 (2023)
34. J.J. Li, A. Sedrakian, M. Alford, Astrophys. J. **944**, 206 (2023)
35. L. Tsaloukidis, P.S. Koliogiannis, A. Kanakis-Pegios, C.C. Moustakidis, Phys. Rev. D **107**, 023012 (2023)
36. P. Danielewicz, R. Lacey, W.G. Lynch, Science **298**, 1592 (2002)
37. B.A. Li, L.W. Chen, C.M. Ko, Phys. Rep. **464**, 113 (2008)
38. B. Friman, C. Höhne, J. Knoll, S. Leupold, J. Randrup, R. Rapp, P. Senger, The CBM physics book: Compressed baryonic matter in laboratory experiments, volume 814. Springer, Berlin (2011)
39. B. Gao, Y. Wang, Z. Gao, Q. Li, Phys. Lett. B **838**, 137685 (2023)
40. D. Bandyopadhyay, S.K. Samaddar, Nucl. Phys. A **484**, 315 (1988)
41. W.D. Myers, W.J. Swiatecki, Ann. Phys. N.Y. **204**, 401 (1990)
42. D. Bandyopadhyay, C. Samanta, S.K. Samaddar, J.N. De, Nucl. Phys. A **511**, 1 (1990)
43. H. Mueller, B.D. Serot, Nucl. Phys. A **606**, 508 (1996)
44. E. Chabanat, P. Bonche, P. Haensel, J. Meyer, R. Schaeffer, Nucl. Phys. A **635**, 231 (1998)
45. K. Strobel, F. Weber, M.K. Weigel, Z. Naturf. A **54**, 83 (1999)
46. D.N. Basu, J. Phys. G **30**, B7 (2004)
47. J. Xu, L.W. Chen, B.A. Li, H.R. Ma, Phys. Rev. C **75**, 014607 (2007)
48. C.C. Moustakidis, Phys. Rev. C **78**, 054323 (2008)
49. H.R. Moshfegh, M. Ghazanfari-Mojarrad, J. Phys. G Nucl. Part. Phys. **38**, 085102 (2011)
50. B. Friedman, V.R. Pandharipande, Nucl. Phys. A **361**, 502 (1981)
51. I.E. Lagaris, V.R. Pandharipande, Nucl. Phys. A **359**, 331 (1981)
52. R.B. Wiringa, V. Fiks, A. Fabrocini, Phys. Rev. C **38**, 1010 (1988)
53. H. Huber, F. Weber, M.K. Weigel, Phys. Rev. C **57**(6), 3484 (1998)
54. A. Akmal, V.R. Pandharipande, D.G. Ravenhall, Phys. Rev. C **58**, 1804 (1998)
55. M. Baldo, A. Fiasconaro, H.Q. Song, G. Giansiracusa, U. Lombardo, Phys. Rev. C **65**, 017303 (2001)
56. T. Frick, H. Müther, Phys. Rev. C **68**, 034310 (2003)
57. A. Fedoseew, H. Lenske, Phys. Rev. C **91**, 034307 (2015)
58. C. Drischler, K. Hebeler, A. Schwenk, Phys. Rev. C **93**, 054314 (2016)
59. M. Lutz, S. Klimt, W. Weise, Nucl. Phys. A **542**, 521 (1992)
60. P. Rehberg, S.P. Klevansky, J. Hüfner, Phys. Rev. C **53**, 410 (1996)
61. T. Hatsuda, T. Kunihiro, Phys. Rep. **247**, 221 (1994)
62. M. Buballa, Phys. Rep. **407**, 205 (2005)
63. M. Ghazanfari Mojarrad, J. Ranjbar, Phys. Rev. C **100**, 015804 (2019)
64. M. Ghazanfari-Mojarrad, J. Ranjbar, Ann. Phys. (N.Y.) **412**, 168048 (2020)
65. H. Liu, J. Xu, C.M. Ko, Phys. Lett. B **803**, 135343 (2020)
66. L.M. Liu, W.H. Zhou, J. Xu, G.X. Peng, Phys. Lett. B **822**, 136694 (2021)
67. J. Ranjbar, M. Ghazanfari Mojarrad, Phys. Rev. C **104**, 045807 (2021)
68. S.A. Ghaemmaghami, M.R. Khoshi, M. Ghazanfari-Mojarrad, Eur. Phys. J. Plus **138**, 1 (2023)

69. W.D. Myers, W.J. Swiatecki, Nucl. Phys. A **601**, 141 (1996)
70. W.D. Myers, W.J. Swiatecki, Phys. Rev. C **57**, 3020 (1998)
71. R.G. Seyler, C.H. Blanchard, Phys. Rev. **124**, 227 (1961)
72. R.G. Seyler, C.H. Blanchard, Phys. Rev. **131**, 355 (1963)
73. J. Randrup, E. Lima-Medeiros, Nucl. Phys. A **529**, 115 (1991)
74. M. Ghazanfari Mojarrad, S.K. Mousavi Khoroshtomi, Int. J. Mod. Phys. E **26**, 1750038 (2017)
75. S.A. Ghaemmaghami, M. Ghazanfari, Mojarrad. Eur. Phys. J. A **58**, 255 (2022)
76. H.R. Moshfegh, M. Ghazanfari-Mojarrad, Eur. Phys. J. A **49**, 1 (2013)
77. M. Ghazanfari-Mojarrad, R. Arabsaeidi, Int. J. Mod. Phys. E **25**, 1650102 (2016)
78. M. Ghazanfari Mojarrad, N.S. Razavi, S. Vaezzade, Nucl. Phys. A **980**, 51 (2018)
79. M. Ghazanfari-Mojarrad, N.S. Razavi, Nucl. Phys. A **986**, 133 (2019)
80. N.S. Razavi, M. Ghazanfari Mojarrad, Nucl. Phys. A **1029**, 122556 (2023)
81. J.M. Lattimer, F. Douglas Swesty, Nucl. Phys. A **535**, 331–376 (1991)
82. C. Constantinou, B. Muccioli, M. Prakash, J.M. Lattimer, Phys. Rev. C **89**, 065802 (2014)
83. C. Constantinou, B. Muccioli, M. Prakash, J.M. Lattimer, Phys. Rev. C **92**, 025801 (2015)
84. Z. Zhang, T. Kunihiro, Phys. Rev. D **80**, 014015 (2009)
85. C.M. Ko, T. Song, F. Li, V. Greco, S. Plumari, Nucl. Phys. A **928**, 234 (2014)
86. C.Q. Guo, H. Liu, J. Xu, Phys. Rev. C **98**, 024914 (2018)
87. H. Liu, F.T. Wang, K.J. Sun, J. Xu, C.M. Ko, Phys. Lett. B **798**, 135002 (2019)
88. R.C. Tolman, Phys. Rev. **55**, 364 (1939)
89. J. Robert-Oppenheimer, G.M. Volkoff, Phys. Rev. **55**, 374 (1939)
90. J.W. Negele, D. Vautherin, Nucl. Phys. A **207**, 298 (1973)
91. G. Baym, C. Pethick, P. Sutherland, Astrophys. J. **170**, 299 (1971)
92. H.T. Cromartie, E. Fonseca, S.M. Ransom, P.B. Demorest, Z. Arzoumanian, H. Blumer, P.R. Brook, M.E. DeCesar, T. Dolch, J.A. Ellis et al., Nat. Astron. **4**, 72 (2020)
93. R. Abbott, T.D. Abbott, S. Abraham, F. Acernese, K. Ackley, C. Adams, R.X. Adhikari, V.B. Adya, C. Affeldt, M. Agathos et al., Astrophys. J. Lett. **896**, L44 (2020)
94. T.E. Riley, A.L. Watts, S. Bogdanov, P.S. Ray, R.M. Ludlam, S. Guillot, Z. Arzoumanian, C.L. Baker, A.V. Bilous, D. Chakrabarty et al., Astrophys. J. Lett. **887**, L21 (2019)
95. M.C. Miller, F.K. Lamb, A.J. Dittmann, S. Bogdanov, Z. Arzoumanian, K.C. Gendreau, S. Guillot, A.K. Harding, W.C.G. Ho, J.M. Lattimer et al., Astrophys. J. Lett. **887**, L24 (2019)
96. J.M. Lattimer, M. Prakash, Science **304**, 536 (2004)